Spin states and persistent currents in a quantum ring with an embedded magnetic impurity

2008 J. Phys.: Condens. Matter 20 025222

(http://iopscience.iop.org/0953-8984/20/2/025222)

IOP PUBLISHING JOURNAL OF PHYSICS: CONDENSED MATTER

J. Phys.: Condens. Matter **20** (2008) 025222 (10pp) doi:10.1088/0953-8984/20/02/025222

Spin states and persistent currents in a quantum ring with an embedded magnetic impurity

J S Sheng and Kai Chang

SKLSM, Institute of Semiconductors, Chinese Academy of Sciences, PO Box 912, Beijing 100083, People's Republic of China

E-mail: kchang@red.semi.ac.cn

Received 26 September 2007, in final form 7 November 2007
Published 13 December 2007
Online at stacks.iop.org/JPhysCM/20/025222

Abstract

Spin states and persistent currents are investigated theoretically in a quantum ring with an embedded magnetic ion under a uniform magnetic field including the spin–orbit interactions. The magnetic impurity acts as a spin-dependent δ-potential for electrons and results in gaps in the energy spectrum, consequently suppressing the oscillation of the persistent currents. The competition between the Zeeman splittings and the s–d exchange interaction leads to a transition of the electron ground state in the ring. The interplay between the periodic potential induced by the Rashba and Dresselhaus spin–orbit interactions and the δ-potential induced by the magnetic impurity leads to significant variation in the energy spectrum, charge density distribution, and persistent currents of electrons in the ring.

(Some figures in this article are in colour only in the electronic version)

1. Introduction

Recently, spin-dependent optical and transport properties of semiconductors have received renewed interest due to the potential applications of spintronic devices [1, 2]. One of the essential requirements in a spintronic device is to generate spin-polarized current. In a diluted magnetic semiconductor (DMS), the s–d exchange interaction [3] between the electrons and the magnetic impurities makes it possible to tailor electron spin splitting and thereby generate spin-polarized currents [4–7].

The spin states of the electrons in a semiconductor can also be manipulated by an external electric field via the spin–orbit interaction (SOI). There are two types of SOI in semiconductors. One is the Rashba spin–orbit interaction (RSOI) induced by structure inversion asymmetry [8, 9], and the other is the Dresselhaus spin–orbit interaction (DSOI) induced by bulk inversion asymmetry [10]. The strength of the RSOI can be tuned by external gate voltages or asymmetric doping, while the strength of the DSOI is inversely proportional to the thickness of the quantum well and thus becomes comparable with that of the RSOI in narrow quantum wells [11]. SOI makes it possible to generate a spin current (SC) electrically without the use of ferromagnetic material or a magnetic field [12, 13]. The impact of in-plane magnetic field on the spin Hall conductivity has been investigated in the two-dimensional electron gas (2DEG) in the presence of both the RSOI and DSOI [14]. The coexistence of the s–d exchange interaction and spin–orbit interactions in 2DEG could result in a significant change of the spin polarization of the charge current (CC) [15].

Recent progress in fabrication techniques makes it possible to dope a few or even one magnetic impurity in a semiconductor nanostructure [16]. Aharonov–Bohm oscillations and spin-polarized transport properties in a quantum open ring with an embedded magnetic impurity have been investigated theoretically [17] using quantum waveguide theory [18] without spin–orbit interactions. Persistent charge and spin currents in closed quantum rings in the presence of a nonmagnetic impurity were studied including the RSOI [19], and a rounding effect of the nonmagnetic impurity on the energy spectrum and the flux oscillation of the persistent CC was found. However, it is interesting to investigate the effect of a magnetic impurity on persistent currents, especially spin current, in a quantum ring. The interplay between the RSOI and DSOI can induce an effective azimuthal periodic potential

in the ring, and consequently breaks the cylindrical symmetry of the ring [20], and this feature makes the spin states and the persistent currents depend sensitively on the position of the magnetic impurity. The impact of Coulomb interaction between electrons in a quantum ring on the energy spectrum and persistent currents should be crucially important and has been investigated theoretically in the absence of the spin–orbit interactions [21–23]. We neglect it here in order to see clearly the effects of the interplay between the spin–orbit interactions and s–d exchange interaction on the single-particle spectrum.

In this work, we study spin states and persistent currents of a 1D quantum ring with an embedded magnetic impurity in the presence of both the RSOI and DSOI. The interplay between the Zeeman splittings and the s–d exchange interaction leads to a transition of the electron ground state. The energy spectrum and the persistent currents depend sensitively on the position of the magnetic impurity including both the RSOI and DSOI, since the interplay between the RSOI and DSOI breaks the cylindrical symmetry. It is interesting to notice that the symmetry of the persistent SC in the parameter space (α–β) is robust against the magnetic impurity. The paper is organized as follows. The theoretical model is presented in section 2. The numerical results and discussion are given in section 3. Finally, we give a brief conclusion in section 4.

2. Theoretical model

In the presence of both the RSOI and DSOI, the dimensionless Hamiltonian of a quantum ring with an embedded magnetic impurity (see figure 1) under a uniform perpendicular magnetic field reads [20]

$$\begin{aligned} H = & \left[-\mathrm{i}\frac{\partial}{\partial\varphi} + \phi + \frac{\alpha}{2}\sigma_\mathrm{r} - \frac{\beta}{2}\sigma_\varphi(-\varphi)\right]^2 \\ & - \frac{\alpha^2+\beta^2}{4} + \frac{\alpha\beta}{2}\sin 2\varphi + g_\mathrm{e}\phi\sigma_z^\mathrm{e} + g_\mathrm{m}\phi\sigma_z^\mathrm{m} \\ & - 2\pi J\,\hat{s}^\mathrm{e}\cdot\hat{s}^\mathrm{m}\delta(\varphi-\theta), \end{aligned} \tag{1}$$

where ϕ is the magnetic flux in the units of $\phi_0 = h/e$, and α and β specify the strengths of the RSOI and DSOI, respectively. $\sigma_\mathrm{r} = \cos\varphi\sigma_x^\mathrm{e} + \sin\varphi\sigma_y^\mathrm{e}$ and $\sigma_\varphi = \cos\varphi\sigma_y^\mathrm{e} - \sin\varphi\sigma_x^\mathrm{e}$, g_e (g_m) is the g factor of the electron (magnetic impurity), and J is the strength of the s–d exchange interaction between the conduction band electron $\hat{s}^\mathrm{e}$ and the magnetic impurity $\hat{s}^\mathrm{m}$. As discussed in our previous work, the interplay between the RSOI and DSOI induces a $\sin 2\varphi$ potential (the third term in equation (1)) and breaks the cylindrical symmetry of the quantum ring [20].

The charge density operator and the charge current density operator are

$$\begin{aligned} \hat{\rho}(\varphi') &= -e\delta(\varphi'-\varphi) \\ \hat{j}_\mathrm{c}(\varphi') &= \tfrac{1}{2}[\hat{\rho}(\varphi')\hat{v} + \hat{v}\hat{\rho}(\varphi')], \end{aligned} \tag{2}$$

where φ' refers to the field coordinates and φ the coordinates of the electron. The velocity operator associated with the Hamiltonian in equation (1) is

$$\hat{v} = \mathbf{e}_\varphi\left[-\mathrm{i}\frac{\partial}{\partial\varphi} + \phi + \frac{\alpha}{2}\sigma_\mathrm{r} - \frac{\beta}{2}\sigma_\varphi(-\varphi)\right]. \tag{3}$$

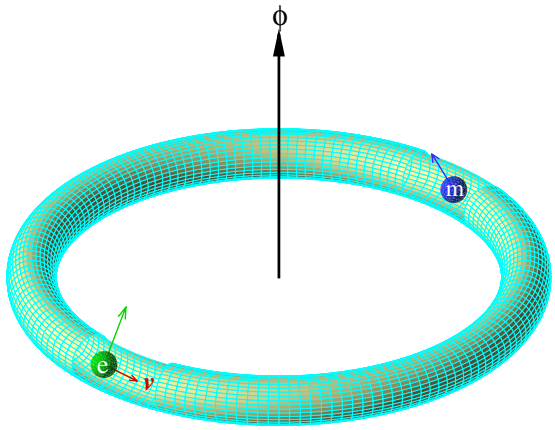

Figure 1. Schematic diagram for a quantum ring with an embedded magnetic impurity.

We can also introduce the spin density and spin current density operators as

$$\begin{aligned} \hat{S}(\varphi') &= \hat{s}^\mathrm{e}\delta(\varphi'-\varphi) \\ \hat{j}_\mathrm{s}(\varphi') &= \tfrac{1}{2}[\hat{S}(\varphi')\hat{v} + \hat{v}\hat{S}(\varphi')], \end{aligned} \tag{4}$$

where $\hat{s}^\mathrm{e}$ is the vector of the electron spin operator. The charge current density and spin current density can be obtained by calculating the expectation values of the corresponding operators:

$$\begin{aligned} j_\mathrm{c}(\varphi') &= \langle\Psi|\hat{j}_\mathrm{c}|\Psi\rangle = -e\,\mathrm{Re}\{\Psi^\dagger(\varphi')\hat{v}'\Psi(\varphi')\} \\ j_\mathrm{s}(\varphi') &= \langle\Psi|\hat{j}_\mathrm{s}|\Psi\rangle = \mathrm{Re}\{\Psi^\dagger(\varphi')\hat{v}'\hat{s}^\mathrm{e}\Psi(\varphi')\}, \end{aligned} \tag{5}$$

where $\Psi(\varphi)$ is the wavefunction of an electron in the ring. For convenience, we denote φ' and $\hat{v}'$ as φ and $\hat{v}$ hereafter.

The azimuthal (spin or charge) current can be defined as [24]

$$I = \frac{1}{2\pi}\int_0^{2\pi} \mathrm{d}\varphi\, j(\varphi). \tag{6}$$

At low temperature, N electrons will occupy the lowest N levels of the energy spectrum. The total (charge or spin) current is the summation over all occupied levels. [19]

3. Numerical results and discussion

3.1. The effects of the magnetic impurity

In order to clearly investigate the effects of the magnetic impurity on the spin states and persistent currents in the 1D ring, we first neglect the Zeeman splittings and spin–orbit interactions. The Hamiltonian of the system becomes

$$H = \left(-\mathrm{i}\frac{\partial}{\partial\varphi} + \phi\right)^2 - 2\pi J\,\hat{s}^\mathrm{e}\cdot\hat{s}^\mathrm{m}\delta(\varphi-\theta). \tag{7}$$

When a spin-1/2 magnetic impurity appears in the quantum ring, the total angular momentum of the eigenstates is equal to 1 (triplet) or 0 (singlet) due to the coupling between

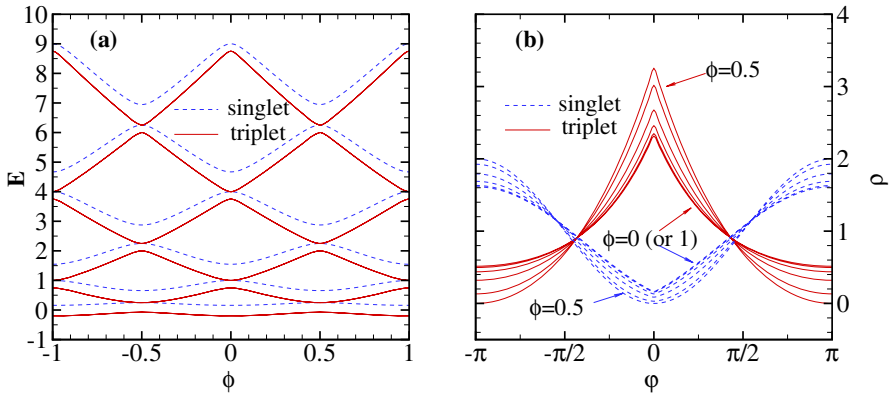

Figure 2. (a) Energy spectrum of a 1D quantum ring with one magnetic impurity at different magnetic fluxes; (b) probability density distribution for the lowest triplet and singlet states of the 1D ring with one magnetic impurity for different magnetic fluxes. $J = 0.5$ and $\theta = 0$.

the electron spin $\hat{s}^{\mathrm{e}}$ and the impurity spin $\hat{s}^{\mathrm{m}}$. In the coupling representation, the Hamiltonian can be written as

$$H_{\mathrm{c}} = \begin{bmatrix} H_{\mathrm{S}} & 0 \\ 0 & H_{\mathrm{T}} I_3 \end{bmatrix}, \tag{8}$$

where $H_{\mathrm{S}} = (-\mathrm{i}\frac{\partial}{\partial\varphi} + \phi)^2 + \frac{3\pi J}{2}\delta(\varphi - \theta)$ is the Hamiltonian for the singlet states ($j = 0$), $H_{\mathrm{T}} = (-\mathrm{i}\frac{\partial}{\partial\varphi} + \phi)^2 - \frac{\pi J}{2}\delta(\varphi - \theta)$ is the Hamiltonian for the triplet states ($j = 1$), and I_3 represents the 3×3 identity matrix. We can find that the magnetic impurity behaves like a barrier (a well) for the singlet (triplet) state when $J > 0$.

Figure 2(a) shows the energy spectrum of the quantum ring with an embedded magnetic impurity. The energy splittings between the triplet and singlet states are proportional to the strength of the exchange interaction $J > 0$. The neighboring singlet and triplet levels can degenerate at special magnetic fluxes (integer or half-integer ϕ). When ϕ is an integer, the energies of the fourfold degenerate levels are $1, 4, 9, \ldots, n^2, \ldots$, which can be obtained from $\sin\pi\kappa = 0$ in both equation (A.6) and equation (A.10) in the appendix; when ϕ is a half-integer, the energies of the fourfold degenerate levels are $1/4, 9/4, 25/4, \ldots, (n + 1/2)^2, \ldots$, which can be obtained from $\cos\pi\kappa = 0$ in both equations (A.7) and (A.11) in the appendix.

Note that the orbital wavefunction and spin wavefunction can be separated in the ring without SOI. The eigenstates of the system can be written as $\Psi = X_{jm}(\varphi)|\frac{1}{2}\frac{1}{2}jm\rangle$ where $j = 0, 1$ and $m = -j, \ldots, j$. The orbital wavefunctions X_{jm} are determined by

$$\begin{aligned} \left(-\mathrm{i}\frac{\partial}{\partial\varphi} + \phi\right)^2 X_{00} + \frac{3}{2}\pi J\delta(\varphi - \theta)X_{00} &= EX_{00}, \\ \left(-\mathrm{i}\frac{\partial}{\partial\varphi} + \phi\right)^2 X_{1m} - \frac{1}{2}\pi J\delta(\varphi - \theta)X_{1m} &= EX_{1m}. \end{aligned} \tag{9}$$

This means that the spin-1/2 magnetic impurity acts as a δ-barrier (well) and well (barrier) on the singlet and triplet states for $J > 0$ ($J < 0$), respectively. This feature consequently leads to different localizations of the singlet and triplet states

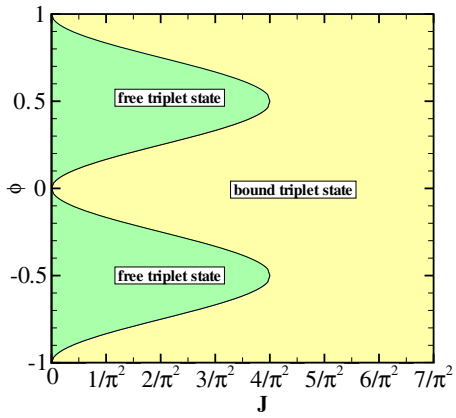

Figure 3. The phase diagram of the ground triplet state in the ring at different magnetic fluxes ϕ and s–d exchange interaction strengths J.

(see figure 2(b)). We assume $J > 0$ in this work without loss of generality. In this case, the ground state of the system is a triplet state.

We now focus on the lowest triplet state. The transition between bound state and free state can be clearly seen in figure 3 as a function of the magnetic flux ϕ and the strength of the s–d exchange interaction J. The lowest triplet state is a bound state at an integer ϕ because equation (A.13) has one solution for any given positive J. Whether the lowest triplet state at a half-integer ϕ is a bound state ($E < 0$) or free state ($E > 0$) depends on the strength of the s–d exchange interaction J. When $J > 4/\pi^2$, equation (A.14) has a nontrivial solution, and therefore the lowest triplet state at a half-integer ϕ is a bound state. When $J < 4/\pi^2$, equation (A.14) only has a trivial solution, and thus the lowest triplet state at a half-integer ϕ is a free state. This means that when the strength of the s–d exchange interaction J is not large enough ($0 < J < 4/\pi^2$) the triplet ground state changes from bound state to free state while varying the magnetic flux ϕ. However, when J is large enough ($J > 4/\pi^2$), the ground state electron is always trapped by the magnetic impurity at any magnetic flux ϕ.

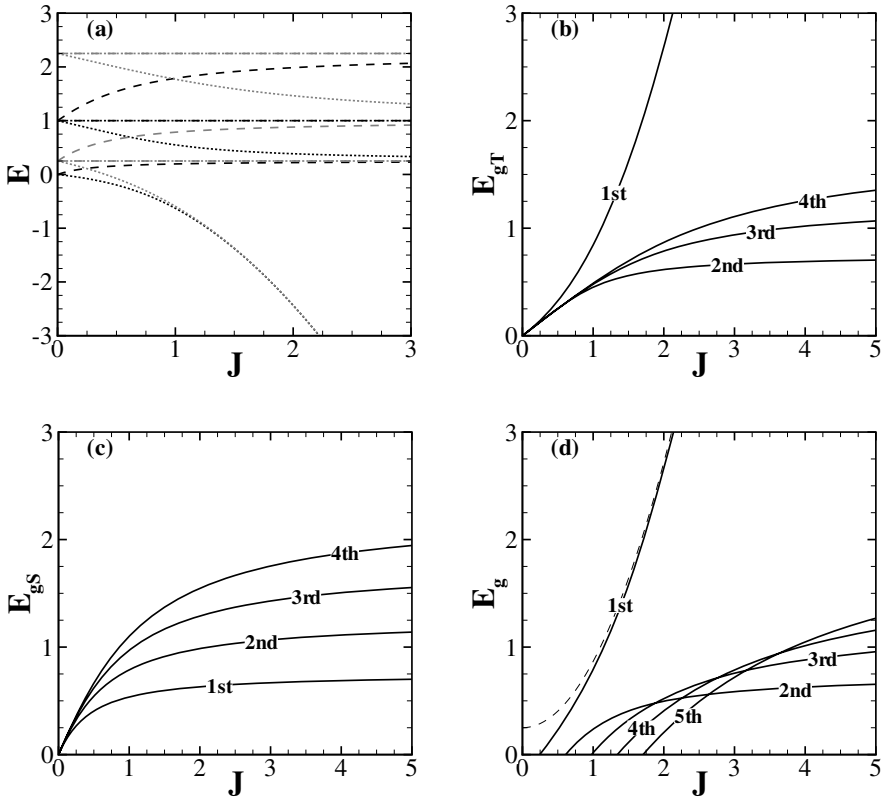

Figure 4. (a) The lowest triplet (dotted) and singlet (dashed) energy levels as functions of the s–d exchange interaction strength J. The dark (gray) lines are for the integer (half-integer) magnetic flux ϕ. (b) The lowest four triplet gaps as functions of J. (c) The lowest four singlet gaps as functions of J. (d) The true energy gaps as functions of the s–d exchange interaction strength J. The dashed line depicts the asymptotic behavior of the lowest energy gap as J increases.

Figure 4(a) depicts the lowest triplet (dotted) and singlet (dashed) energy levels as functions of the strength of the s–d exchange interaction J at an integer magnetic flux (dark) or half-integer magnetic flux (gray). The dash–dotted horizontal lines correspond to those special fourfold degenerate points in figure 2(a) whose energies do not change with J. The energy difference of two triplet (or singlet) states at different magnetic fluxes but of the same order approach zero as $J \to \infty$, e.g.,

$$E_{\mathrm{T1}}(\phi = 0) \to E_{\mathrm{T1}}(\phi = 1/2) \to -\pi^2 J^2/16$$

$$E_{\mathrm{S1}}(\phi = 0) \to E_{\mathrm{S1}}(\phi = 1/2) = 1/4$$

$$E_{\mathrm{T2}}(\phi = 0) \to E_{\mathrm{T2}}(\phi = 1/2) = 1/4$$

$$E_{\mathrm{S2}}(\phi = 1/2) \to E_{\mathrm{S2}}(\phi = 0) = 1$$

$$E_{\mathrm{T3}}(\phi = 1/2) \to E_{\mathrm{T3}}(\phi = 0) = 1$$

as $J \to \infty$. These results can be obtained from approximate solutions to the three transcendental equations, i.e. (A.5), (A.9) and (A.12) in the appendix, for large J at integer and half-integer magnetic flux. The lowest four energy gaps between triplet (singlet) states are shown in figure 4(b) (4(c)). But they are only pseudo-gaps. The true gaps are shown in figure 4(d); the energy gaps appear successively and increase as J increases. The lowest energy gap $E_{\mathrm{g1}} = E_{\mathrm{S1}}(\phi = 0) - E_{\mathrm{T1}}(\phi = 1/2)$ approaches $1/4 + \pi^2 J^2/16$ as $J \to \infty$ (see the dashed line in figure 4(d)), and the second lowest energy gap $E_{\mathrm{g2}} = E_{\mathrm{S2}}(\phi = 1/2) - E_{\mathrm{T2}}(\phi = 0)$ approaches $1 - 1/4 = 3/4$ as $J \to \infty$. The third, fourth, and fifth lowest energy gaps approach $5/4$, $7/4$, and $9/4$ as $J \to \infty$, respectively.

Figure 5(a) shows the persistent CCs from the lowest triplet and singlet energy levels at different magnetic flux ϕ. The persistent CCs from both the triplet and singlet states are smoothed and suppressed by the magnetic impurity. The persistent SCs from the lowest $|1, -1\rangle$, $|1, 0\rangle$, $|1, 1\rangle$, and $|0, 0\rangle$ are depicted in figure 5(b). The SC contributions of $|1, 0\rangle$ and $|0, 0\rangle$ are always zero and the SC contributions of $|1, -1\rangle$ and $|1, 1\rangle$ are always opposite, thus canceling each other. We note that the persistent SC from the lowest $|1, -1\rangle$ is proportional to the persistent CC from the same state. The oscillation amplitudes, i.e. the maximal values, of the persistent CCs from the lowest triplet and singlet energy levels are shown in figure 5(c) with different strengths of the s–d exchange interaction J. The persistent CCs from both the lowest triplet and singlet energy levels decline as J increases. We recall that the magnetic impurity acts as a δ-well (δ-barrier) for the triplet (singlet) states. Both the δ-well and δ-barrier hinder electron propagation along the ring and suppress the persistent CCs (and SCs). The persistent CC from the lowest triplet energy level declines more rapidly than its singlet counterpart because the electron is more localized (around the δ-well) for

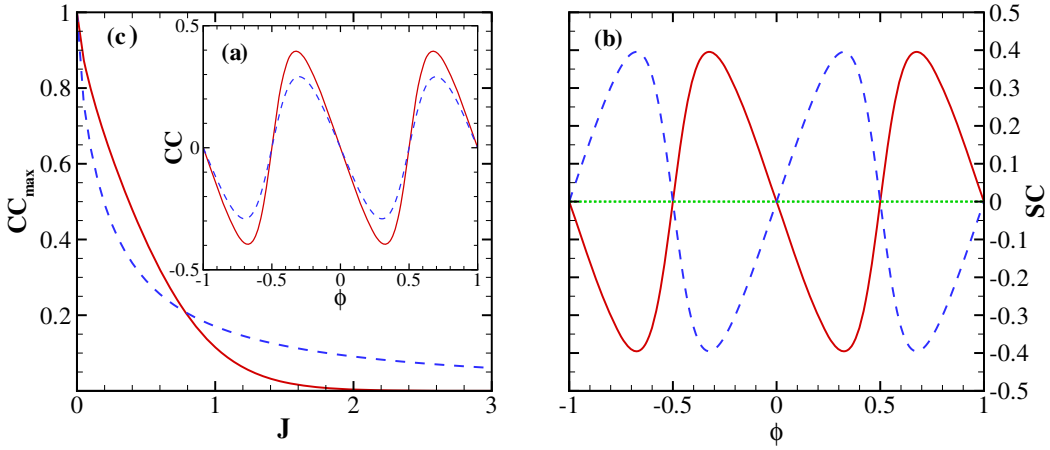

Figure 5. (a) The persistent CC from the lowest triplet (singlet) energy level at different magnetic fluxes ϕ is denoted by the red solid (blue dashed) line, $J = 0.5$; (b) the persistent SC from the lowest $|1, -1\rangle$ ($|1, 1\rangle$) state is denoted by the red solid (blue dashed) line, and the green dotted lines are the persistent SC from the lowest $|1, 0\rangle$ state and that from the lowest $|0, 0\rangle$ state, $J = 0.5$; (c) the maximal value of the persistent CC from the lowest triplet (singlet) energy level with different strengths of the s–d exchange J is denoted by a red solid (blue dashed) line.

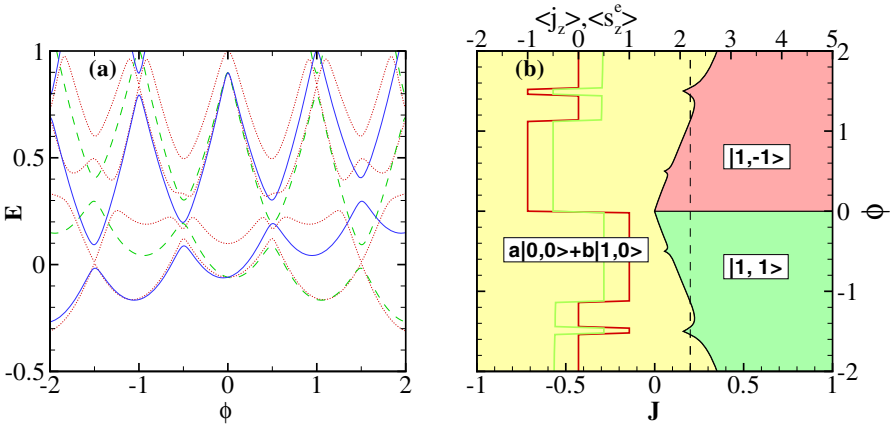

Figure 6. (a) Energy spectrum of a GaAs ring with an embedded spin-1/2 magnetic impurity ($J = 0.2$); the Zeeman terms of both the electron and the magnetic impurity are included, $g_e = -0.029\,48$ and $g_m = 0.134$; the red dotted lines denote those levels with zero $\langle \hat{j}_z \rangle$, and the green dashed (blue solid) lines denote the $|1, -1\rangle$ ($|1, 1\rangle$) levels; (b) the three-phase transition of the ground state, and the variations of $\langle \hat{j}_z \rangle$ (the red (dark) line) and $\langle \hat{s}_z \rangle$ (the green (gray) line) along the dashed line ($J = 0.2$), $\bar{g}_1 = -0.02948$ and $\bar{g}_2 = 0.134$.

the triplet states than for the singlet states. Nevertheless, for small J the persistent CC from the lowest singlet energy level can be smaller than that from the lowest triplet energy level (see figure 5(a)) because the strength of the δ-barrier for the singlet states is triple the strength of the δ-well for the triplet states.

Now we include the intrinsic Zeeman terms of both the electron and the magnetic impurity, e.g. GaAs ring. The energy spectrum with an embedded spin-1/2 magnetic impurity is depicted in figure 6(a). The dimensionless g factors $g_e = g_e^* m^* = -0.029\,48$ and $g_m = g_m^* m^* = 0.134$. It is interesting to notice that the $|0, 0\rangle$ states and $|1, 0\rangle$ states are coupled together by the Zeeman terms (see equation (A.16)). Although these states are mixed, the projection of the angular momentum along the z-axis $\langle \hat{j}_z \rangle$ is still a good quantum number, i.e. $\langle \hat{j}_z \rangle = 0$ (see the red dotted lines in figure 6(a)). The states $|1, -1\rangle$ and $|1, 1\rangle$ are decoupled, and the Zeeman terms only alter their energies (see the green dashed lines and the blue solid lines in figure 6(a)), while the total spin $\hat{j}$ and its z-component $\hat{j}_z$ are still good quantum numbers. Figure 6(b) shows the phase diagram for the ground state of the ring at different J and ϕ. From this figure one can see that the ground state in the ring can transit among these three kinds of states due to the interplay between the Zeeman terms and s–d exchange interaction as the magnetic flux ϕ increases, and $\langle \hat{j}_z \rangle$ and $\langle \hat{s}_z \rangle$ undergo sudden changes across boundaries in the phase diagram (see the red (dark) and green (gray) lines in figure 6(b)).

3.2. The effects of the RSOI and DSOI

In this subsection, we focus on the competition between the s–d exchange interaction and SOIs. From equation (1), the interplay between the RSOI and DSOI induces a $\sin 2\varphi$ periodic potential and breaks the cylindrical symmetry of the

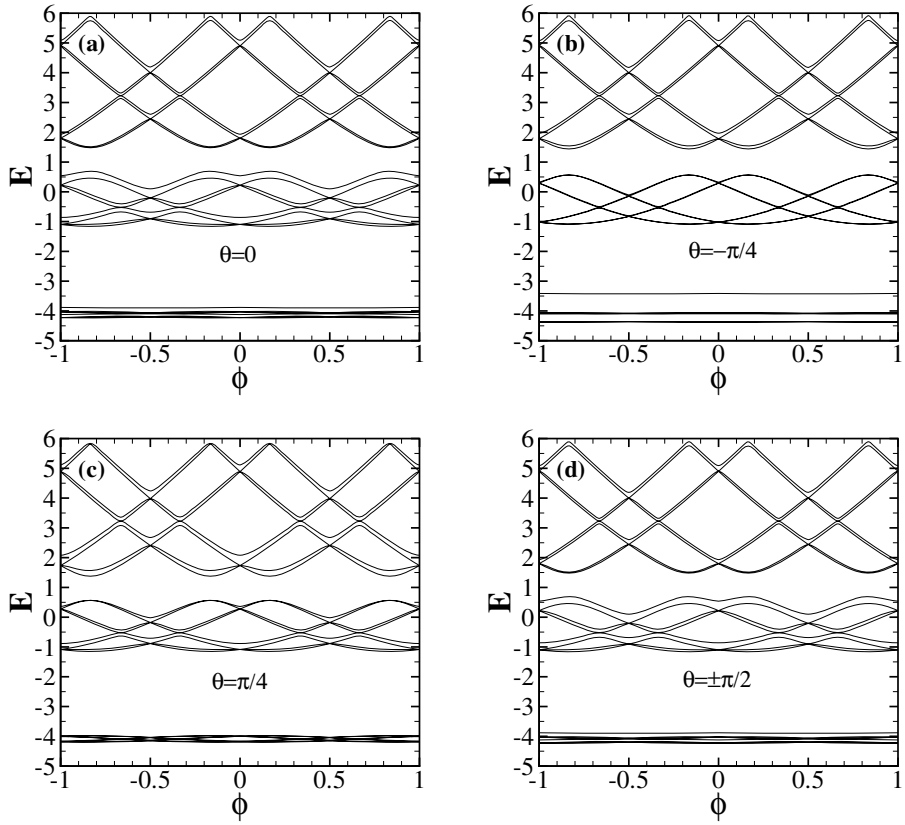

Figure 7. Energy spectrum of 1D quantum ring with an embedded spin-1/2 magnetic impurity and two types of SOI, $J = 0.2$, $\alpha = 3$ and $\beta = 2$; the position of the impurity is $\theta = 0$ in panel (a), and $-\pi/4$, $\pi/4$, $\pm\pi/2$ in panel (b), (c), (d) respectively.

quantum ring. The spin states, energy spectrum and persistent currents depend sensitively on the position of the magnetic impurity.

Figure 7 depicts the influence of the position of the magnetic impurity on the eigenenergy spectrum of the quantum ring in the presence of both the RSOI and DSOI. Strictly speaking, the degeneracy of the triplet states is lifted by the RSOI and DSOI. The position of the magnetic impurity more significantly influences the lower energy levels than the higher levels since the wavefunctions of the lower states are more localized than that of the higher states. In such an anisotropic ring, $\theta = 0$ and $\pm\pi/2$ are equivalent positions which can be connected to each other by mirror reflections with respect to the $\varphi = \pm\pi/4$ planes, and therefore two energy spectra in panels (a) and (d) in figure 7 are exactly the same. The energy splittings due to the s–d exchange interaction in panel (b) ((c)) are largest (smallest) because the probability density of the lowest bound states exhibits maxima (minima) when the magnetic impurity is located at the bottom (peak) of the $\sin 2\varphi$ periodic potential induced by the interplay between the RSOI and DSOI. We also notice that the corresponding energy splittings of the second bound state in panel (b) are zero because the magnetic impurity is located just at the node ($\theta = -\pi/4$) of the wavefunction of the second bound state.

Figure 8 shows the probability density distributions of the lowest singlet and triplet states for different positions of the magnetic impurity. The electron is distributed along the ring according to the potential $\frac{\alpha\beta}{2}\sin 2\varphi$, which is induced by the interplay between the RSOI and DSOI (see equation (1)) in the absence of a magnetic impurity. This potential $\frac{\alpha\beta}{2}\sin 2\varphi$ exhibits two valleys at $\varphi = -\pi/4$ and $3\pi/4$, where the electron is most likely to appear, and two peaks at $\varphi = \pi/4$ and $-3\pi/4$, corresponding to the minimum of the probability density of the electron. As shown in the previous subsection, the magnetic impurity acts as a δ-like barrier for the singlet state electron and as a δ-well for the triplet state electron when $J > 0$, and the height of the δ-barrier is three time larger than that of the δ-well (see equation (9)). Thus the presence of the magnetic impurity will make the potential profile at the positions $\varphi = -\pi/4$ and $3\pi/4$ no longer equivalent. From figure 8 one can find that the competition between the magnetic impurity and SOIs, i.e. the probability density of an electron at one of the two valleys, is enhanced (reduced) for the triplet (singlet) state electron when the position of the magnetic impurity approaches the valley. It is interesting to note that the magnetic impurity acting as a δ-like barrier for the singlet state could also enhance the probability density of the electron at the other valley $\varphi = 3\pi/4$ when it approaches the valley $\varphi = -\pi/4$ of the potential $\frac{\alpha\beta}{2}\sin 2\varphi$.

Two types of energy gaps appear in the energy spectrum of a quantum ring, including the RSOI, the DSOI, and the s–d exchange interaction (see figure 9). In our previous work [20], we discussed the energy gaps caused by the coexistence of the RSOI and DSOI ($E_{\text{g-I}}$). As shown in figure 4(d), the s–d exchange interaction can also open an energy gap ($E_{\text{g-II}}$) if the strength J is greater than the corresponding threshold

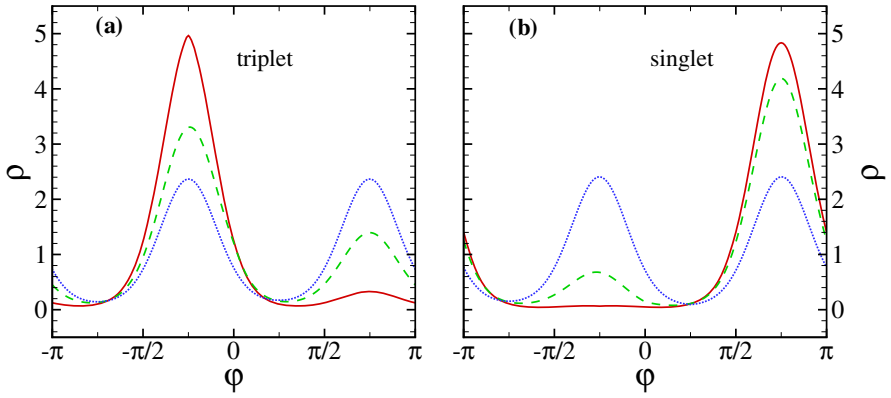

Figure 8. The probability density distributions of the lowest triplet (panel (a)) and singlet (panel (b)) states. The red solid (green dashed, blue dotted) line is for the magnetic impurity located at $\theta = -\pi/4$ $(0, \pi/4)$. Other parameters are $J = 0.2$, $\alpha = 3$, $\beta = 2$, and $\phi = 0$.

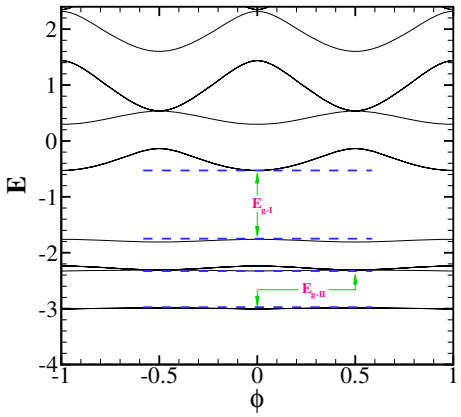

Figure 9. Two types of energy gaps appear in the energy spectrum while the spin–orbit interactions and s–d exchange interaction coexist in the quantum ring. $E_{\text{g-I}}$ denotes the lowest (direct) energy gap induced by the RSOI and DSOI; $E_{\text{g-II}}$ denotes the lowest (indirect) energy gap induced by the s–d exchange interaction. $\alpha = \beta = 2$, $J = 1, \theta = 0$.

value. We demonstrate in figure 10 that the two types of energy gaps tend to compete against each other. The lowest SOI induced gap declines as the strength of the s–d exchange interaction increases (see figure 10(a)). This is because the energy splittings between singlet and triplet states caused by the s–d exchange interaction tend to squeeze the gap induced by SOI especially when the magnetic impurity approaches the valley of potential ($\theta = -\pi/4$) since the s–d exchange interaction is a contact interaction that depends on the overlap between the magnetic impurity and the electron. Figure 10(b) depicts the energy gap induced by the s–d exchange interaction as a function of the strength of SOIs. The increasing strengths of the RSOI and DSOI enhance the localization of the electron. The gap increases when the magnetic impurity is located at the valley of the potential $\frac{\alpha\beta}{2}\sin 2\varphi$ ($\theta = -\pi/4$) as the SOI strengths (α and β) increase, or decrease when the magnetic impurity is at other sites. The gap width decreases most rapidly when the magnetic impurity is located at the peak of the potential $\frac{\alpha\beta}{2}\sin 2\varphi$ ($\theta = \pi/4$).

The s–d exchange interaction can also influence the persistent SC. In figure 11(a), we show a contour plot of the persistent SC as a function of the s–d exchange interaction strength J and the position of the magnetic impurity θ. We can see that the persistent SC oscillates with the magnetic impurity position θ when the strength J is fixed. The magnitude of the persistent SC exhibits maxima at $\theta = \pi/4, 3\pi/4, 5\pi/4, 7\pi/4$, where the valleys and peaks of the potential $\frac{\alpha\beta}{2}\sin 2\varphi$ are. There are also four specific positions of magnetic impurity (the white regions in figure 11(a)) where the magnitude of the persistent SC exhibits minima. These positions are determined by the specific strengths of the RSOI and DSOI. When the magnetic impurity is at a peak (valley) of the potential $\frac{\alpha\beta}{2}\sin 2\varphi$, the magnitude of the persistent SC increases (decreases) as the s–d exchange interaction strength J increases. This provides us with a possible way to control the spin current utilizing the magnetic impurity.

We depict the persistent SC with different RSOI strength α and DSOI strength β in figure 11(b) at a fixed J. The symmetry of the persistent SC in the α–β parameter space is still the same as what we reported before in the absence of the magnetic impurity [20]. The eigenenergy levels become twofold degenerate when α and β are tuned to proper values in the absence of the magnetic impurity, and the contributions from these two degenerate levels cancel each other and consequently lead to the vanishing SC. This twofold degeneracy will be lifted by the s–d exchange interaction and the levels split into singlet and triplet states. The contributions to the persistent SC from the singlet states ($|0, 0\rangle$) are zero while those from the triplet states ($|1, -1\rangle$, $|1, 0\rangle$, $|1, 1\rangle$) states cancel each other so that the total persistent SC is still zero even in the presence of the magnetic impurity. This is why the symmetry is robust against the magnetic impurity. But the magnitude of the persistent SC is suppressed by the magnetic impurity, i.e. the s–d exchange interaction.

4. Conclusions

We have investigated theoretically the spin states and persistent currents (CC and SC) in a 1D ring with an embedded magnetic impurity. The s–d exchange interaction between the electron and the magnetic impurity splits the eigenstates into singlet

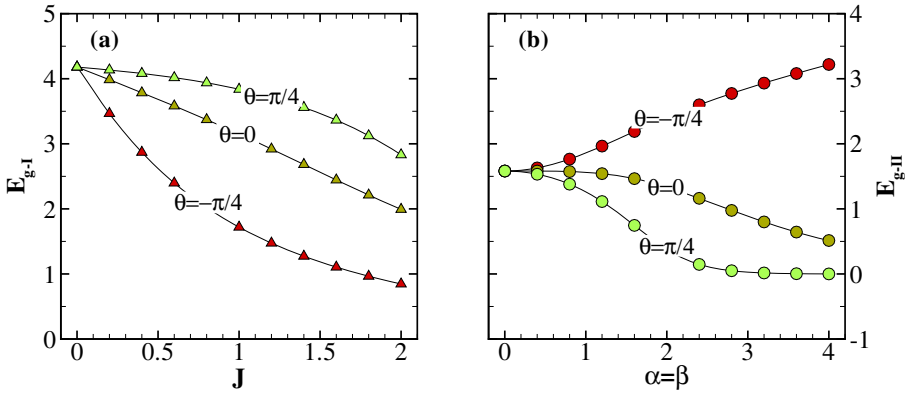

Figure 10. (a) The lowest SOI induced gap versus the s–d exchange interaction strength J with different positions of the magnetic impurity, $\alpha = \beta = 3$; (b) the lowest s–d induced gap versus the SOI strengths ($\alpha = \beta$) with different positions of the magnetic impurity, $J = 1.5$.

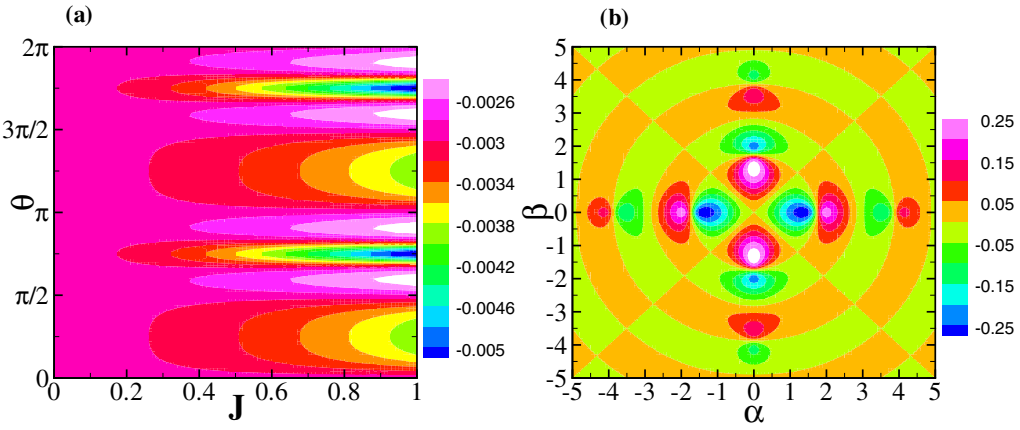

Figure 11. (a) Contour plot of the persistent SC as a function of the strength J of the s–d exchange interaction and the impurity position θ, $\alpha = 3$, $\beta = 2$, and $\phi = 0.5$; (b) contour plot of the persistent SC as a function of the RSOI strength α and DSOI strength β, $J = 0.5$, $\theta = 0$, and $\phi = 0.5$.

states and triplet states. The magnetic impurity acts as a δ-barrier (δ-well) for the singlet (triplet) states when $J > 0$, opens energy gaps in the energy spectrum, and suppresses the persistent CC and SC. The competition between the Zeeman terms and the s–d exchange interaction leads to a transition of the electron ground state in the ring. The eigenenergy spectrum, probability distribution, and persistent SC depend sensitively on the position of the magnetic impurity. The symmetry of the persistent SC in parameter space (α–β) is not destroyed by the magnetic impurity.

Acknowledgments

This work was supported by the NSFC grant no. 60525405 and the knowledge innovation project of CAS.

Appendix. The Hamiltonian in the coupling representation

In the decoupling representation, the basis set is the direct product of the spin states of the electron and the magnetic impurity $|s_z^{\mathrm{e}}\rangle \bigotimes |s_z^{\mathrm{m}}\rangle$. The Hamiltonian of a one-dimensional ring with an embedded magnetic impurity can be written as

$$H_{\mathrm{nc}} = \begin{array}{c} \\ |\downarrow\downarrow\rangle \\ |\uparrow\downarrow\rangle \\ |\downarrow\uparrow\rangle \\ |\uparrow\uparrow\rangle \end{array} \begin{array}{c} \begin{array}{cccc} |\downarrow\downarrow\rangle & |\uparrow\downarrow\rangle & |\downarrow\uparrow\rangle & |\uparrow\uparrow\rangle \end{array} \\ \begin{bmatrix} H_- & 0 & 0 & 0 \\ 0 & H_+ & -\pi J\delta(\varphi-\theta) & 0 \\ 0 & -\pi J\delta(\varphi-\theta) & H_+ & 0 \\ 0 & 0 & 0 & H_- \end{bmatrix} \end{array}, \tag{A.1}$$

where $H_+ = (-\mathrm{i}\frac{\partial}{\partial\varphi} + \phi)^2 + \frac{\pi J}{2}\delta(\varphi-\theta)$ and $H_- = (-\mathrm{i}\frac{\partial}{\partial\varphi} + \phi)^2 - \frac{\pi J}{2}\delta(\varphi-\theta)$. We can transform it to the coupling representation via a unitary operator S which is related to C–G coefficients $S^{\frac{1}{2}\frac{1}{2}}_{\mathrm{m}_1 m_2 jm}$.

$$H_{\mathrm{c}} = S^{-1} H_{\mathrm{nc}} S,$$

$$S = \begin{array}{c} \\ |\downarrow\downarrow\rangle \\ |\uparrow\downarrow\rangle \\ |\downarrow\uparrow\rangle \\ |\uparrow\uparrow\rangle \end{array} \begin{array}{c} \begin{array}{cccc} |0,\ 0\rangle & |1,-1\rangle & |1,\ 0\rangle & |1,\ 1\rangle \end{array} \\ \begin{bmatrix} 0 & 1 & 0 & 0 \\ 1/\sqrt{2} & 0 & 1/\sqrt{2} & 0 \\ -1/\sqrt{2} & 0 & 1/\sqrt{2} & 0 \\ 0 & 0 & 0 & 1 \end{bmatrix} \end{array},$$

$$S^{-1} = S'. \tag{A.2}$$

Thus the Hamiltonian in the coupling representation is

$$H_{\mathrm{c}} = \begin{bmatrix} H_{\mathrm{S}} & 0 \\ 0 & H_{\mathrm{T}} I_3 \end{bmatrix}, \tag{A.3}$$

where $H_{\mathrm{S}} = (-\mathrm{i}\frac{\partial}{\partial\varphi}+\phi)^2+\frac{3\pi J}{2}\delta(\varphi-\theta)$ is the Hamiltonian for the singlet states ($j=0$), $H_{\mathrm{T}} = (-\mathrm{i}\frac{\partial}{\partial\varphi}+\phi)^2-\frac{\pi J}{2}\delta(\varphi-\theta)$ is the Hamiltonian for the triplet states ($j=1$), and I_3 represents the 3×3 identity matrix.

Because of the cylindrical symmetry, the position of the magnetic impurity can be assumed to be $\theta = 0$ without loss of generality.

For the singlet state, the magnetic impurity acts as a δ-potential barrier whose strength is $\frac{3\pi J}{2}$ ($J>0$). All related eigenstates should be free states in the ring ($E=\kappa^2>0, \kappa>0$), and can be determined by

$$\begin{gathered}\left(-\mathrm{i}\frac{\partial}{\partial\varphi}+\phi\right)^2 X = \kappa^2 X, \qquad 0<\varphi<2\pi \\ X(0) = X(2\pi) \\ X'(0)-X'(2\pi) = \frac{3\pi J}{2}X(0).\end{gathered} \tag{A.4}$$

The general solution $X(\varphi) = C_1\mathrm{e}^{\mathrm{i}(\kappa-\phi)\varphi} + C_2\mathrm{e}^{-\mathrm{i}(\kappa+\phi)\varphi}$; we obtain the following transcendental equation:

$$4\kappa[\cos 2\pi\phi - \cos 2\pi\kappa] = 3\pi J \sin 2\pi\kappa. \tag{A.5}$$

The singlet eigenenergies $E=\kappa^2$ can be obtained from the zeros of equation (A.5). We further consider the following special cases.

(a) When ϕ is an integer: the κ values are determined by

$$\sin\pi\kappa = 0 \qquad \text{or} \qquad \cot\pi\kappa = \frac{4\kappa}{3\pi J}. \tag{A.6}$$

(b) When ϕ is a half-integer: the κ values are determined by

$$\cos\pi\kappa = 0 \qquad \text{or} \qquad \tan\pi\kappa = -\frac{4\kappa}{3\pi J}. \tag{A.7}$$

For the triplet state electrons, the magnetic impurity acts as a δ-potential well whose strength is $\frac{\pi J}{2}$ ($J>0$). The lowest triplet state could be a bound state ($E=-\kappa^2<0, \kappa>0$), and the higher states can still be free states extended over the whole ring ($E=\kappa^2>0, \kappa>0$). The free triplet eigenstates can be determined by

$$\begin{gathered}\left(-\mathrm{i}\frac{\partial}{\partial\varphi}+\phi\right)^2 X = \kappa^2 X, \qquad 0<\varphi<2\pi \\ X(0) = X(2\pi) \\ X'(0)-X'(2\pi) = -\frac{\pi J}{2}X(0).\end{gathered} \tag{A.8}$$

The corresponding transcendental equation can be derived similarly,

$$4\kappa[\cos 2\pi\phi - \cos 2\pi\kappa] = -\pi J \sin 2\pi\kappa. \tag{A.9}$$

The eigenenergy spectra at the specific magnetic fluxes are the following.

(a) When ϕ is an integer: the κ values are determined by

$$\sin\pi\kappa = 0 \qquad \text{or} \qquad \cot\pi\kappa = -\frac{4\kappa}{\pi J}. \tag{A.10}$$

(b) When ϕ is a half-integer: the κ values are determined by

$$\cos\pi\kappa = 0 \qquad \text{or} \qquad \tan\pi\kappa = \frac{4\kappa}{\pi J}. \tag{A.11}$$

The triplet bound state can be obtained by substituting κ with $\mathrm{i}\kappa$ in equations (A.8)–(A.11). The corresponding transcendental equation is

$$4\kappa[\cos 2\pi\phi - \cosh 2\pi\kappa] = -\pi J \sinh 2\pi\kappa. \tag{A.12}$$

The eigenenergy spectra at the specific magnetic fluxes are the following.

(a) When ϕ is an integer: the κ values are determined by

$$\coth\pi\kappa = \frac{4\kappa}{\pi J}. \tag{A.13}$$

(b) When ϕ is a half-integer: the κ values are determined by

$$\tanh\pi\kappa = \frac{4\kappa}{\pi J}. \tag{A.14}$$

The Zeeman terms are diagonal matrix elements in decoupling representation,

$$H_{\mathrm{nc}}^Z = \begin{bmatrix} -(g_{\mathrm{e}}+g_{\mathrm{m}})\phi & 0 & 0 & 0 \\ 0 & (g_{\mathrm{e}}-g_{\mathrm{m}})\phi & 0 & 0 \\ 0 & 0 & (g_{\mathrm{m}}-g_{\mathrm{e}})\phi & 0 \\ 0 & 0 & 0 & (g_{\mathrm{e}}+g_{\mathrm{m}})\phi \end{bmatrix}. \tag{A.15}$$

But in coupling representation this becomes

$$H_{\mathrm{c}}^Z = S^{-1}H_{\mathrm{nc}}^Z S = \begin{bmatrix} 0 & 0 & (g_{\mathrm{e}}-g_{\mathrm{m}})\phi & 0 \\ 0 & -(g_{\mathrm{e}}+g_{\mathrm{m}})\phi & 0 & 0 \\ (g_{\mathrm{e}}-g_{\mathrm{m}})\phi & 0 & 0 & 0 \\ 0 & 0 & 0 & (g_{\mathrm{e}}+g_{\mathrm{m}})\phi \end{bmatrix}. \tag{A.16}$$

Generally speaking, g_{e} is not equal to g_{m}, and therefore the singlet $|0,0\rangle$ and triplet $|1,0\rangle$ states are coupled together by the Zeeman terms (see $(g_{\mathrm{e}}-g_{\mathrm{m}})\phi$ in equation (A.16)).

References

[1] Wolf S A, Awschalom D D, Buhrman R A, Daughton J M, von Molnár S, Roukes M L, Chtchelkanova A Y and Treger D M 2001 Spintronics: a spin-based electronics vision for the future *Science* **294** 1488–95

[2] Žutić I, Fabian J and Das Sarma S 2004 Spintronics: fundamentals and applications *Rev. Mod. Phys.* **76** 323

[3] Furdyna J K 1988 Diluted magnetic semiconductors *J. Appl. Phys.* **64** R29–64

[4] Fiederling R, Keim M, Reuscher G, Ossau W, Schmidt G, Waag A and Molenkamp L W 1999 Injection and detection of a spin-polarized current in a light-emitting diode *Nature* **402** 787–90

[5] Ohno Y, Young D K, Beschoten B, Matsukura F, Ohno H and Awschalom D D 1999 Electrical spin injection in a ferromagnetic semiconductor heterostructure *Nature* **402** 790–2

[6] Jaroszyński J, Wróbel J, Sawicki M, Kamińska E, Skośkiewicz T, Karczewski G, Wojtowicz T, Piotrowska A, Kossut J and Dietl T 1995 Influence of s–d exchange interaction on universal conductance fluctuations in $Cd_{1-x}Mn_xTe$:In *Phys. Rev. Lett.* **75** 3170–3

[7] Sawicki M, Dietl T, Kossut J, Igalson J, Wojtowicz T and Plesiewicz W 1986 Influence of s–d exchange interaction on the conductivity of $Cd_{1-x}Mn_xSe$:In in the weakly localized regime *Phys. Rev. Lett.* **56** 508–11

[8] Rashba E I 1960 Properties of semiconductors with an extremum loop. 1. Cyclotron and combinational resonance in a magnetic field perpendicular to the plane of the loop *Sov. Phys.—Solid State* **2** 1109

[9] Bychkov Y A and Rashba E I 1984 Oscillatory effects and the magnetic-susceptibility of carriers in inversion-layers *J. Phys. C: Solid State Phys.* **17** 6039

[10] Dresselhaus G 1955 Spin–orbit coupling effects in zinc-blende structures *Phys. Rev.* **100** 580

[11] Lommer G, Malcher F and Rössler U 1988 Spin splitting in semiconductor heterostructures for $B \to 0$ *Phys. Rev. Lett.* **60** 728–31

[12] Murakami S, Nagaosa N and Zhang S C 2003 Dissipationless quantum spin current at room temperature *Science* **301** 1348–51

[13] Sinova J, Culcer D, Niu Q, Sinitsyn N A, Jungwirth T and MacDonald A H 2004 Universal intrinsic spin Hall effect *Phys. Rev. Lett.* **92** 126603

[14] Chang M C 2005 Effect of in-plane magnetic field on the spin Hall effect in a Rashba–Dresselhaus system *Phys. Rev.* B **71** 085315

[15] Yang W, Chang K, Wu X G and Zheng H Z 2006 Interplay between s–d exchange interaction and Rashba effect: spin-polarized transport *Appl. Phys. Lett.* **89** 132112

[16] Besombes L, Leger Y, Maingault L, Ferrand D, Mariette H and Cibert J 2004 Probing the spin state of a single magnetic ion in an individual quantum dot *Phys. Rev. Lett.* **93** 207403

[17] Joshi S K, Sahoo D and Jayannavar A M 2001 Aharonov–Bohm oscillations and spin-polarized transport in a mesoscopic ring with a magnetic impurity *Phys. Rev.* B **64** 075320

[18] Xia J B 1992 Quantum wave-guide theory for mesoscopic structures *Phys. Rev.* B **45** 3593–9

[19] Splettstoesser J, Governale M and Zülicke U 2003 Persistent current in ballistic mesoscopic rings with Rashba spin–orbit coupling *Phys. Rev.* B **68** 165341

[20] Sheng J S and Chang K 2006 Spin states and persistent currents in mesoscopic rings: spin–orbit interactions *Phys. Rev.* B **74** 235315

[21] Gudmundsson V, Tang C S and Manolescu A 2003 Nonadiabatic current generation in a finite width semiconductor ring *Phys. Rev.* B **67** 161301

[22] Gylfadottir S S, Nita M, Gudmundsson V and Manolescu A 2005 Net current generation in a 1D quantum ring at zero magnetic field *Physica* E **27** 278–83

[23] Gylfadottir S S, Harju A, Jouttenus T and Webb C 2006 Interacting electrons on a quantum ring: exact and variational approach *New J. Phys.* **8** 211

[24] Wendler L, Fomin V M and Krokhin A A 1994 Relation between persistent current and band-structure of finite-width mesoscopic rings *Phys. Rev.* B **50** 4642–7